

Goal-Oriented Semantic Communication for ISAC-Enabled Robotic Obstacle Avoidance

Wenjie Liu, Yansha Deng, *Senior Member, IEEE*, and Henk Wymeersch, *Fellow, IEEE*

Abstract—Obstacle avoidance is a fundamental task in mobile robotics and has been extensively studied over the past decades. However, existing studies are fundamentally limited by an exclusive reliance on robot’s onboard sensors, which restricts the field of view and lacks the global understanding of dynamic environments. How to leverage the base station (BS) to enable sensing and control of mobile robots for reliable obstacle avoidance remains largely underexplored. To fill this gap, we investigate an integrated sensing and communication (ISAC)-enabled BS for the unmanned aerial vehicle (UAV) obstacle avoidance task, and propose a goal-oriented semantic communication (GOSC) framework for the BS to transmit sensing and command and control (C&C) signals efficiently and effectively. Our GOSC framework establishes a closed loop for sensing–C&C generation–sensing and C&C transmission: For sensing, a Kalman filter (KF) is applied to continuously predict UAV positions, mitigating the reliance of UAV position acquisition on continuous sensing signal transmission, and enhancing position estimation accuracy through sensing–prediction fusion. Based on the refined estimation position provided by the KF, we develop a Mahalanobis distance-based dynamic window approach (MD-DWA) to generate precise C&C signals under uncertainty, in which we derive the mathematical expression of the minimum Mahalanobis distance required to guarantee collision avoidance. Finally, for efficient sensing and C&C signal transmission, we propose an effectiveness-aware deep Q-network (E-DQN) to determine the transmission of sensing and C&C signals based on their value of information (VoI). The VoI of sensing signals is quantified by the reduction in uncertainty entropy of UAV’s position estimation, while the VoI of C&C signals is measured by their contribution to UAV navigation improvement. Extensive simulations validate the effectiveness of our proposed GOSC framework. Compared to the conventional ISAC transmission framework that transmits sensing and C&C signals at every time slot, GOSC achieves the same 100% task success rate while reducing the number of transmitted sensing and C&C signals by 92.4% and the number of transmission time slots by 85.5%.

Index Terms—Goal-oriented semantic communication, sensing and communication, robotic obstacle avoidance, Kalman filter, Mahalanobis distance, and value of information.

I. INTRODUCTION

OBSTACLE avoidance is one of the fundamental tasks in mobile robotics, which aims at navigating a robot towards its destination without collisions in environments populated with obstacles [1]. Over the past decades, it has been extensively studied due to its broad applications in areas such

as autonomous vehicles, unmanned aerial vehicles (UAVs), service robotics, and industrial automation. Broadly, existing studies on robotic obstacle avoidance can be classified into two categories: multi-sensor fusion approaches [2] and collision-avoidance algorithmic approaches [3]. The former focuses on integrating data from multiple onboard sensors—such as cameras, inertial measurement units (IMUs), and LiDARs—in efficient ways to provide richer environmental information that supports navigation decision-making [4]. The latter emphasizes the design of more sophisticated obstacle avoidance algorithms, leveraging techniques from control theory, optimization, and artificial intelligence (AI) to enhance navigation safety and efficiency [5].

However, a common limitation of existing mobile robot obstacle avoidance research is that the environmental perception is based solely on robot’s onboard sensors, which inherently leads to two drawbacks: a restricted sensing range of each robot that prevents global environmental awareness, and the challenge in effective coordination among multiple robots via global view. Integrated sensing and communication (ISAC) [6] is a promising technique to overcome these two drawbacks. With ISAC, the base station (BS) can act as a global coordinator of multiple robots, providing a global view and control. This can be achieved by transmitting sensing signals to detect the positions of robots and environmental obstacles; based on the sensed positions, the BS could subsequently generate and transmit command-and-control (C&C) signals via downlink communication to specify the robots’ movement.

As an emerging technique, ISAC has attracted increasing attention in recent years. However, existing studies on ISAC is primarily limited to the sensing and single link communication performance optimization, e.g., channel capacity [7], energy consumption [8], mean-square-error (MSE) [9], Cramér-Rao bound (CRB) [10], and the inherent trade-off between sensing and communication [11]. The research question of “How should the BS jointly design sensing and C&C signals to control robots for safe and reliable obstacle avoidance” remains largely unexplored. A commonly adopted approach in the existing ISAC literature is to transmit ISAC signals continuously [12]. Nevertheless, this strategy presents a critical drawback: ensuring safe navigation requires the ISAC signals to be transmitted at each time slot with a high frequency, which results in high communication and computation costs. Notably, when there are no obstacles in the vicinity of the robots, continuous ISAC transmission yields redundant information and unnecessary resource consumption.

Goal-oriented semantic communication (GOSC) [13] has recently been recognized as a promising paradigm to address

Wenjie Liu and Yansha Deng are with the Department of Engineering, King’s College London, Strand, London WC2R 2LS, U.K. (e-mail: wenjie.liu@kcl.ac.uk; yansha.deng@kcl.ac.uk) (Corresponding author: Yansha Deng).

Henk Wymeersch is with the Department of Electrical Engineering, Chalmers University of Technology, Gothenburg, Sweden (e-mail: henkw@chalmers.se).

the redundant transmission problem. Unlike conventional bit-oriented communication schemes that aim to transmit all signals reliably at the bit level, GOSC focuses on extracting and transmitting the task-relevant information from the raw data, enabling more efficient and purpose-driven information exchange. By doing so, it can significantly reduce the communication size while guaranteeing the success of the task. Recent efforts have explored the application of GOSC in robotic control: Xu *et al.* [14] defined semantic-level and effectiveness-level performance metrics for C&C signals, and designed a general task-oriented semantic-aware framework to reduce the redundant transmission of C&C signals. Wu *et al.* [15] proposed a joint age of information (AoI) and value of information (VoI) based queue ranking strategy to prioritize those effectiveness-critical C&C signals received by the UAV. However, [14] and [15] focused solely on the transmission of C&C signals under the ideal assumption that the BS knows the accurate location of UAV in real-time. This assumption is unrealistic in practice since sensing inevitably introduces detection errors. While in the context of ISAC, the transmission of C&C signals inherently depends on the accuracy of sensing results. This intrinsic coupling between sensing and communication highlights the necessity to jointly design the GOSC transmission for both sensing and C&C signals.

Motivated by the above, the main contributions of this work are summarized as follows:

- We consider an ISAC-enabled BS for the UAV obstacle avoidance task, in which the BS transmits sensing signals to detect the UAV's position, and transmits C&C signals to control the movements of UAV to fly towards the destination while avoiding dynamic obstacles. Our goals are twofold: to enable the UAV to complete the task as quickly as possible, and to minimize the communication sizes of transmitted sensing and C&C signals.
- We propose a GOSC framework for ISAC-enabled robotic obstacle avoidance, aiming to achieve effective sensing and C&C signal transmission. Our GOSC framework consists of a closed loop for sensing–C&C generation–sensing and C&C transmission to enable the BS to transmit sensing and C&C signals efficiently and effectively:
 - 1) For sensing, we apply a Kalman filter (KF) to continuously predict the UAV's position based on the most recently transmitted C&C signals, which enables the BS to acquire a reference position of the UAV without the needs to transmit sensing signals. When a sensing signal is transmitted, it can also fuse sensing and prediction results to provide a more accurate position estimation of the UAV.
 - 2) Based on the UAV position provided by the KF, we propose a Mahalanobis distance-based dynamic window approach (MD-DWA) to generate precise C&C signals under estimation uncertainty. In particular, we derive the mathematical expression of the minimum Mahalanobis distance to avoid collision.
 - 3) We design an effectiveness-aware deep Q-network

(E-DQN) to determine whether to transmit sensing and C&C signals based on their VoI. The VoI of sensing signals is quantified by the reduction of uncertainty entropy of UAV's position estimation, while the VoI of C&C signals is measured by the improvement in UAV navigation.

- Extensive simulations validate the effectiveness of our proposed GOSC framework. Compared to the traditional ISAC transmission framework that transmits sensing and C&C signals at every time slot, GOSC achieves the same 100% task success rate while reducing the number of transmitted sensing and C&C signals by 92.4% and the required transmission time slots by 85.5%.

The rest of this paper is organized as follows. Section II presents the system model and problem formulation; Section III introduces a traditional ISAC signal transmission framework; Section IV describes our proposed GOSC framework; Section V presents simulation results and analysis; and Section VI concludes the paper.

Notation. Unless otherwise specified, we denote column vectors as bold lowercase italics (e.g., \mathbf{a}), matrices as bold uppercase italics, (e.g., \mathbf{A}), and constants as uppercase letters, (e.g., A). The i -th element of a vector and the (i, j) -th element of a matrix are denoted by $[\mathbf{a}]_i$ and $[\mathbf{A}]_{i,j}$, respectively. The Euclidean norm is represented by $\|\cdot\|$, and the Mahalanobis distance by $\|\cdot\|_M$. The transpose, conjugate, and inverse of a matrix are denoted by $(\cdot)^T$, $(\cdot)^*$ and $(\cdot)^{-1}$, respectively. The Gaussian distribution is denoted as \mathcal{N} , while the complex Gaussian distribution is denoted as \mathcal{CN} . The operator \odot represents element-wise multiplication. A column vector of ones is denoted as $\mathbf{1}$, and a column vector of zeros is denoted as $\mathbf{0}$. The identity matrix of size $N \times N$ is denoted as \mathbf{I}_N , and a zero matrix of size $N \times N$ is denoted as $\mathbf{0}_N$.

II. SYSTEM MODEL AND PROBLEM FORMULATION

In this section, we provide a brief introduction to the ISAC-enabled BS for the UAV obstacle avoidance task. We then describe the sensing and C&C signal transmission and reception. Next, the kinematic models of the UAV and obstacles are presented, followed by the beamforming model. Finally, a problem is formulated with the aim to transmit sensing and C&C signals.

A. Scenario Description

As shown in Fig. 1, we consider an ISAC-enabled BS for the UAV obstacle avoidance task, where the BS sends sensing signals to detect the position of UAV, which is then used to generate and transmit C&C signals. The C&C signals specify UAV's speed and heading angle to guide it flying towards the destination while avoiding dynamic obstacles. The whole task period can be discretised into I time slots, and the time slot index is denoted as t_i , where $i \in \{0, 1, 2, \dots, I\}$ and the time slot interval $\Delta t = t_{i+1} - t_i$ ($\forall i$) is a constant. Without loss of generality, we assume the UAV flies in the $x - y$ plane at a fixed altitude H . The real horizontal position of UAV at t_i is denoted as $\mathbf{p}(t_i) = [p_x(t_i), p_y(t_i)]^T$. Note that the BS can not obtain the real position of UAV $\mathbf{p}(t_i)$, and can only

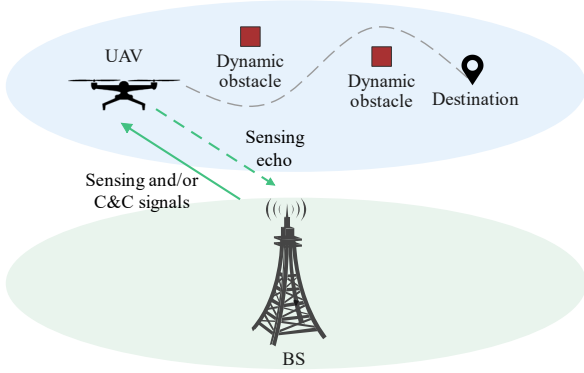


Fig. 1: ISAC-enabled BS for the UAV obstacle avoidance task.

send sensing signal to detect the position of UAV. The detected horizontal position is denoted as $\hat{\mathbf{p}}(t_i) = [\hat{p}_x(t_i), \hat{p}_y(t_i)]^T$. We assume that the horizontal positions of obstacles are detected by other cooperative BSs. The real and detected obstacle positions are denoted as $\mathbf{p}_o(t_i)$ and $\hat{\mathbf{p}}_o(t_i)$, respectively, where $o \in \{1, 2, 3, \dots, N_o\}$ and N_o is the total number of obstacles. Due to the thermal noise and quantization noise, there are always detection errors between the real position and the detected position, both for the UAV and obstacles [16]. Under such detection errors, our goal is to design an efficient and reliable joint sensing and C&C transmission scheme that enables the UAV to avoid dynamic obstacles and reach its destination as quickly as possible.

B. Sensing and C&C Signal Transmission Models

We consider a mono-static multiple-input multiple-output (MIMO) system, in which the BS uses the same antenna array to transmit millimeter wave (mmWave) sensing and/or C&C signals and receive sensing echoes. We assume that the BS is equipped uniform linear array (ULA) with K antennas, which transmit orthogonal frequency division multiplexing (OFDM) signal across M subcarriers with a subcarrier spacing Δf . The antenna element spacing is $D = \lambda_c/2$, where λ_c is the carrier wavelength. The OFDM signal has a symbol duration of $T_{\text{sym}} = T_{\text{cp}} + T_c$, where T_{cp} is the cyclic prefix (CP) duration and $T_c = 1/\Delta f$ is the elementary OFDM symbol duration. The complex baseband OFDM signal for sensing at instant time t within the t_i -th time slot can be denoted as

$$\mathbf{x}_i^s(t) = \frac{1}{\sqrt{M}} \sum_{m=0}^{M-1} z_m^s e^{j2\pi m \Delta f (t-t_i)} \text{rect}\left(\frac{t-t_i}{T_{\text{sym}}}\right), \quad (1)$$

where z_m^s is the complex sensing symbol mapped on the m -th subcarrier and $\mathbb{E}\{|z_m^s|^2\} = 1$, $\text{rect}(\cdot)$ is the rectangular function and is defined as

$$\text{rect}(x) \triangleq \begin{cases} 1, & 0 \leq x \leq 1, \\ 0, & \text{otherwise.} \end{cases} \quad (2)$$

We assume that the C&C data is modulated into N_{cc} symbols via quadrature phase shift keying (QPSK), the complex

downlink baseband OFDM signal at instant time t within the t_i -th time slot can be denoted as

$$\mathbf{x}_i^c(t) = \frac{1}{\sqrt{M}} \sum_{m=0}^{M-1} \sum_{n=0}^{N_{\text{cc}}-1} \eta_{m,n} z_n^c(t_i) e^{j2\pi m \Delta f (t-t_i)} \text{rect}\left(\frac{t-t_i}{T_{\text{sym}}}\right), \quad (3)$$

where $z_n^c(t_i)$ is the n -th complex C&C symbol at t_i and $\mathbb{E}\{|z_n^c(t_i)|^2\} = 1$, $\eta_{m,n} \in \{0, 1\}$ denotes whether mapping the n -th C&C symbol on the m -th subcarrier. It should be mentioned that sensing typically requires a large bandwidth to achieve high-resolution detection, while transmitting the C&C signals only consumes a rather small bandwidth. In other words, M is much greater than N_{cc} . Thus, we use $\eta_{m,n}$ to map C&C symbols multiple times across M subcarriers to enhance communication reliability. The complex baseband transmit signal at t_i is expressed as

$$\mathbf{x}_i^{\text{tx}}(t) = \delta_s(t_i) \mathbf{x}_i^s(t) + \delta_c(t_i) \mathbf{x}_i^c(t), \quad (4)$$

where $\delta_s(t_i)$ and $\delta_c(t_i)$ are binary variables that indicate whether to transmit sensing and communication baseband signals, respectively. For clarity, if the BS transmits both sensing and C&C signals within one time slot, we denote the combined signal as ‘ISAC signal’. Here, it is important to note that the generation of C&C signals depends on the sensing detection results. Without loss of generality, we assume that it takes one time slot for the BS to receive the sensing echo, process the sensing data, and generate the corresponding C&C signal. The C&C signal can be transmitted in the subsequent time slot. Thus, $\delta_s(t_i)$ and $\delta_c(t_i)$ are defined as

$$\delta_s(t_i) \triangleq \begin{cases} 1, & \text{transmitting sensing signal at the} \\ & \text{beginning of } t_i, \\ 0, & \text{otherwise,} \end{cases} \quad (5)$$

$$\delta_c(t_i) \triangleq \begin{cases} 1, & \text{if sensing signal is transmitted at } t_{i-1} \\ & \text{and C\&C signal is transmitted at the} \\ & \text{beginning of } t_i, \\ 0, & \text{otherwise.} \end{cases} \quad (6)$$

C. Sensing Receiver Signal Model

Since the positions of obstacles are provided by the cooperative BSs, we focus solely on the reflected signal from the UAV. Practical experiments have shown that the UAV can easily establish a light-of-sight (LoS) link with the BS [17], thus only a single direct reflection path between the BS and the UAV is considered in the sensing process. Specifically, the BS transmits a sensing signal at the beginning of the t_i -th time slot, which is reflected by the UAV and received by the BS within the same slot. Since the UAV’s velocity is controlled by the BS and known a priori, the Doppler shift induced by its motion can be regarded as constant during one time slot and effectively compensated using appropriate parameterization techniques [18]. After signal sampling and applying an M -point fast Fourier transform (FFT), the received sensing echo at the BS in the frequency domain can be expressed as [19]

$$\mathbf{Y}_s(t_i) = \sqrt{\frac{P}{M}} \xi(t_i) \mathbf{a}_{\text{rx}}(\theta(t_i)) \mathbf{a}_{\text{tx}}^T(\theta(t_i)) \mathbf{f}(t_i) \cdot [\mathbf{x}_s \odot \boldsymbol{\mu}(\tau_s(t_i))]^T + \mathbf{Z}, \quad (7)$$

where P is the transmit power, $\xi(t_i) = \sqrt{\frac{\sigma_{\text{RCS}} \lambda_c^2}{(4\pi)^3 r^4(t_i)}}$ represents the attenuation coefficient, in which σ_{RCS} is the radar cross section (RCS) of the UAV, $r(t_i)$ is the Euclidean distance from the UAV to the BS at t_i , $\mathbf{f}(t_i) \in \mathbb{C}^{K \times 1}$ is the beamforming vector and discussed in *Subsection F*, $\mathbf{x}_s = [z_0^s, z_1^s, \dots, z_{M-1}^s]^\top$, $\boldsymbol{\mu}(\tau_s(t_i)) \in \mathbb{C}^{M \times 1}$ is the phase shift across OFDM subcarriers, in which each element can be expressed as $[\boldsymbol{\mu}(\tau_s(t_i))]_m = e^{-j2\pi m \Delta f \tau_s(t_i)}$, $\tau_s(t_i) = \frac{2r(t_i)}{c_0}$ is the round trip delay, $\mathbf{Z} \in \mathbb{C}^{K \times M}$ is the additive noise and each entry $[\mathbf{Z}]_{k,m} \sim \mathcal{CN}(0, \Delta f \sigma_0^2)$, σ_0^2 is the power spectral density of additive white Gaussian noise (AWGN), $\mathbf{a}_{\text{rx}}(\theta(t_i)) \in \mathbb{C}^{K \times 1}$ and $\mathbf{a}_{\text{tx}}(\theta(t_i)) \in \mathbb{C}^{K \times 1}$ are steering vectors of receiver and transmitter, respectively, which are denoted as

$$\begin{aligned} \mathbf{a}_{\text{rx}}(\theta(t_i)) &= \mathbf{a}_{\text{tx}}(\theta(t_i)) \\ &= \left[1, e^{-j2\pi \frac{D \sin(\theta(t_i))}{\lambda_c}}, \dots, e^{-j2\pi \frac{(K-1)D \sin(\theta(t_i))}{\lambda_c}} \right]^\top. \end{aligned} \quad (8)$$

Since the BS has access to the complex baseband signal \mathbf{x}_s in advance, we can remove its impact on the sensing receiver signal $\mathbf{Y}_s(t_i)$ via zero-forcing reciprocal filtering [20]. The filtered signal is written as

$$\tilde{\mathbf{Y}}_s(t_i) = \sqrt{P} \xi(t_i) \mathbf{a}_{\text{rx}}(\theta(t_i)) \mathbf{a}_{\text{tx}}^\top(\theta(t_i)) \mathbf{f}(t_i) \boldsymbol{\mu}^\top(\tau_s(t_i)) + \mathbf{Z}. \quad (9)$$

After obtaining $\tilde{\mathbf{Y}}_s(t_i)$, we adopt multiple signal classification (MUSIC) algorithm [21] and parabolic interpolation of FFT (PIFFT) algorithm [22] to acquire the angle of arrival (AoA) $\hat{\theta}(t_i)$ and distance $\hat{r}(t_i)$, respectively. The detection variance of $\hat{\theta}(t_i)$ can be given by [23]

$$\sigma^2(\theta(t_i)) \approx \frac{6}{\text{SNR}_s(t_i) \pi^2 \cos^2(\theta(t_i)) K^3}, \quad (10)$$

where $\text{SNR}_s(t_i)$ is the sensing signal-to-noise ratio (SNR) across K antennas at t_i and is denoted as

$$\text{SNR}_s(t_i) = \frac{KP(\xi(t_i))^2 |\mathbf{a}_{\text{tx}}^\top(\theta(t_i)) \mathbf{f}(t_i)|^2}{M \Delta f \sigma_0^2}. \quad (11)$$

The detection variance of distance $\hat{r}(t_i)$ is given as [24]

$$\sigma^2(r(t_i)) \approx \left(\frac{c_0}{2M \Delta f} \right)^2 \frac{1}{16\pi^2 \text{SNR}_s(t_i)}. \quad (12)$$

The relationship between the real AoA $\theta(t_i)$, distance $r(t_i)$ and their detected AoA $\hat{\theta}(t_i)$, distance $\hat{r}(t_i)$ are denoted as

$$\begin{cases} \hat{\theta}(t_i) = \theta(t_i) + \epsilon_\theta(t_i), \\ \hat{r}(t_i) = r(t_i) + \epsilon_r(t_i), \end{cases} \quad (13)$$

where $\epsilon_\theta(t_i) \sim \mathcal{N}(0, \sigma^2(\theta(t_i)))$ and $\epsilon_r(t_i) \sim \mathcal{N}(0, \sigma^2(r(t_i)))$ are detection errors of AoA and distance, respectively. The real, detection positions of UAV in 2D Cartesian coordination and their relationship are represented as

$$\begin{cases} \mathbf{p}(t_i) = \begin{bmatrix} r(t_i) \cos(\theta(t_i)), & r(t_i) \sin(\theta(t_i)) \end{bmatrix}^\top, \\ \hat{\mathbf{p}}(t_i) = \begin{bmatrix} \hat{r}(t_i) \cos(\hat{\theta}(t_i)), & \hat{r}(t_i) \sin(\hat{\theta}(t_i)) \end{bmatrix}^\top, \\ \hat{\mathbf{p}}(t_i) = \mathbf{p}(t_i) + [\epsilon_x(t_i), \epsilon_y(t_i)]^\top. \end{cases} \quad (14)$$

Lemma 1. The detection errors $\epsilon_x(t_i)$ and $\epsilon_y(t_i)$ in 2D Cartesian coordination can be derived as

$$\begin{bmatrix} \epsilon_x(t_i) \\ \epsilon_y(t_i) \end{bmatrix} \approx \mathbf{J}(t_i) \begin{bmatrix} \epsilon_r(t_i) \\ \epsilon_\theta(t_i) \end{bmatrix}, \quad (15)$$

where $\mathbf{J}(t_i)$ is the Jacobian matrix of $\mathbf{p}(t_i)$ evaluated at $(\hat{r}(t_i), \hat{\theta}(t_i))$.

Proof. Please see Appendix A. \square

According to **Lemma 1**, the detection position variances $\sigma_x^2(t_i)$ and $\sigma_y^2(t_i)$ of the UAV in 2D Cartesian coordination can be denoted as

$$\begin{aligned} \sigma_x^2(t_i) &= \cos^2(\theta(t_i)) \sigma^2(r(t_i)) + r^2(t_i) \sin^2(\theta(t_i)) \times \\ &\quad \sigma^2(\theta(t_i)), \\ \sigma_y^2(t_i) &= \sin^2(\theta(t_i)) \sigma^2(r(t_i)) + r^2(t_i) \cos^2(\theta(t_i)) \times \\ &\quad \sigma^2(\theta(t_i)). \end{aligned} \quad (16)$$

D. Communication Receiver Signal Model

We consider a rotary-wing UAV equipped with one receive antenna. The wireless channel is modeled as

$$\mathbf{h}(t_i) = \sqrt{\beta(t_i)} \mathbf{g}(t_i), \quad (17)$$

where $\mathbf{h}(t_i) \in \mathbb{C}^{K \times 1}$, $\beta(t_i)$ is the large-scale fading, $\mathbf{g}(t_i) \in \mathbb{C}^{K \times 1}$ is the small-scale fading. Since the wireless channel between the BS and the UAV is dominated by the LoS link, the free-space path loss model [25] is used to describe the large-scale fading

$$\beta(t_i) = \left(\frac{\lambda_c}{4\pi r(t_i)} \right)^2. \quad (18)$$

Similarly, due to the existence of LoS link, the small-scale fading is modeled by the Rician fading below [17]

$$\begin{aligned} \mathbf{g}(t_i) &= \sqrt{\frac{\kappa}{\kappa+1}} \mathbf{a}_{\text{tx}}(\theta(t_i)) \alpha_0 \delta(\zeta - \zeta_0) \\ &\quad + \sqrt{\frac{1}{\kappa+1}} \sum_{q=1}^{Q-1} \alpha_q \delta(\zeta - \zeta_q), \end{aligned} \quad (19)$$

where κ is the Rician factor, α_0 is the deterministic LoS channel component with $|\alpha_0| = 1$, ζ_0 is the delay on LoS channel, $\delta(\cdot)$ is Dirac delta function, α_q denotes non-line-of-sight (NLoS) fading component, $\alpha_q \sim \mathcal{CN}(0, \sigma_q^2)$ and $\sum_q \sigma_q^2 = 1$, ζ_q is the delay on the q -th NLoS channel, Q is the total number of transmission paths. As noted in equation (3), we assume the C&C symbols are repeatedly mapped L times across M subcarriers. The maximum ratio combining (MRC) [26] is adopted at the UAV side to make full use of frequency diversity gain. Thus, the communication SNR between the BS and the UAV at the t_i -th time slot can be expressed as

$$\text{SNR}_c(t_i) = \frac{P\beta(t_i)}{M \Delta f \sigma_0^2} \sum_{l=1}^L \left| \mathbf{g}_l^\top(t_i) \mathbf{f}(t_i) \right|^2, \quad (20)$$

where $\mathbf{g}_l(t_i)$ is a realization of $\mathbf{g}(t_i)$ at the l -th mapping subcarriers. The latency for transmitting the C&C data can be denoted as

$$\tau_c(t_i) = \frac{2L N_{\text{cc}}}{M \Delta f \log_2(1 + \text{SNR}_c(t_i))}. \quad (21)$$

Due to the LoS channel and the application of MRC, we assume that the UAV can successfully receive and decode the the C&C data within the same time slot, i.e., $\tau_c(t_i) < \Delta t$ ($\forall t_i$).

E. UAV Kinematic Model

At every time slot, the forward angle $\phi(t_i)$ and speed $V(t_i)$ of the UAV are controlled by the C&C signal. Specifically, if the C&C signal is transmitted at the t_i -th time slot, the UAV executes its corresponding command $\phi(t_i)$ and $V(t_i)$; otherwise, the UAV adopts the command from the last time slot $\phi(t_{i-1})$ and $V(t_{i-1})$, which can be written as

$$\begin{cases} V(t_i) = \delta_c(t_i)V(t_i) + (1 - \delta_c(t_i))V(t_{i-1}), \\ \phi(t_i) = \delta_c(t_i)\phi(t_i) + (1 - \delta_c(t_i))\phi(t_{i-1}). \end{cases} \quad (22)$$

Due to propulsion limitations of the UAV, the maximum changes in angle and speed within one time slot are $\Delta\phi$ and ΔV , respectively; the maximum flying speed can not exceed V_{\max} . Thus, the commanded values should satisfy

$$\begin{cases} |V(t_i) - V(t_{i-1})| \leq \Delta V, \quad V(t_i) \in [0, V_{\max}], \\ |\phi(t_i) - \phi(t_{i-1})| \leq \Delta\phi, \quad \phi(t_i) \in [0, 2\pi]. \end{cases} \quad (23)$$

Based on the C&C signal, the kinematic model of the UAV can be given as

$$\begin{cases} p_x(t_{i+1}) = p_x(t_i) + V(t_{i-1}) \cos(\phi(t_{i-1}))\tau_c(t_i) + \\ \quad V(t_i) \cos(\phi(t_i))(\Delta t - \tau_c(t_i)) + \eta_x(t_i), \\ p_y(t_{i+1}) = p_y(t_i) + V(t_{i-1}) \sin(\phi(t_{i-1}))\tau_c(t_i) + \\ \quad V(t_i) \sin(\phi(t_i))(\Delta t - \tau_c(t_i)) + \eta_y(t_i), \end{cases} \quad (24)$$

where $\eta_x(t_i), \eta_y(t_i) \sim \mathcal{N}(0, \sigma_\eta^2)$ are Gaussian noise due to environmental disturbance or system imperfection.

F. Beamforming Model

The beampattern synthesis approach in [27] is adopted to design the beamforming vector $\mathbf{f}(t_i)$ for sensing and communication. Specifically, we construct an uniform angular grid covering $[-\frac{\pi}{2}, \frac{\pi}{2}]$, which consists of N_ϑ discrete grid points denoted by $\{\vartheta_u\}_{u=1}^{N_\vartheta}$. Given the detected AoA $\hat{\theta}(t_i)$ and variance $\sigma^2(\hat{\theta}(t_i))$, we define the scope of the direction from the BS towards the UAV at time t_i as $\vartheta_{\text{CI}}(t_i) = [\vartheta_{\min}(t_i), \vartheta_{\max}(t_i)]$, where the boundary angles are given as

$$\begin{cases} \vartheta_{\min}(t_i) = \hat{\theta}(t_i) - B\sigma(\hat{\theta}(t_i)), \\ \vartheta_{\max}(t_i) = \hat{\theta}(t_i) + B\sigma(\hat{\theta}(t_i)), \end{cases} \quad (25)$$

in which B is the confidence level factor. Let $\mathbf{b}_D(t_i) \in \mathbb{C}^{N_\vartheta \times 1}$ denote the desired beam pattern over the angular grid. Its entries are defined as

$$[\mathbf{b}_D(t_i)]_u \triangleq \begin{cases} K, & \text{if } \vartheta_u \in \vartheta_{\text{CI}}(t_i), \\ 0, & \text{otherwise.} \end{cases} \quad (26)$$

The beam pattern synthesis problem can be formulated as

$$\min_{\mathbf{f}(t_i)} \|\mathbf{b}(t_i) - \mathbf{A}_{\text{tx}}^\top \mathbf{f}(t_i)\|^2 \quad (27)$$

where $\mathbf{A}_{\text{tx}}^\top = [\mathbf{a}_{\text{tx}}(\vartheta_1), \dots, \mathbf{a}_{\text{tx}}(\vartheta_{N_\vartheta})] \in \mathbb{C}^{K \times N_\vartheta}$ denotes the transmit steering matrix evaluated at the grid points. This least squares problem has a closed-form solution

$$\mathbf{f}(t_i) = (\mathbf{A}_{\text{tx}}^* \mathbf{A}_{\text{tx}}^\top)^{-1} \mathbf{A}_{\text{tx}}^* \mathbf{b}_D(t_i). \quad (28)$$

G. Obstacle Kinematic Model and Detection Model

Dynamic obstacles are randomly distributed along the flight route of the UAV. The kinematic model of any obstacle can be denoted as

$$\begin{cases} p_{ox}(t_{i+1}) = p_{ox}(t_i) + V_{ox}(t_i)\Delta t, \\ p_{oy}(t_{i+1}) = p_{oy}(t_i) + V_{oy}(t_i)\Delta t, \end{cases} \quad (29)$$

where $V_{ox}(t_i), V_{oy}(t_i)$ are the obstacle velocities along the x - and y -axes, respectively, which are not known in advance. Due to the uncertainty of obstacle locations and movements, the cooperative BSs need to detect obstacle positions at each time slot. The detailed detection process is not the focus of this work. Instead, we leverage the detected obstacle positions and their uncertainties at each time slot. For safety, the cooperative BSs scan the surrounding environment within a circular region centered at the UAV. Accordingly, the set of obstacles detected at time t_i can be expressed as

$$\hat{\mathcal{O}}(t_i) = \{o \mid \|\mathbf{p}_o(t_i) - \hat{\mathbf{p}}(t_i)\| \leq R_{\text{scan}}\}, \quad (30)$$

in which R_{scan} is the scanning radius. Let $\epsilon_{ox}(t_i)$ and $\epsilon_{oy}(t_i)$ denote the detection errors of obstacles along the x - and y -axes at time t_i . These errors are modeled as Gaussian random variables

$$\epsilon_{ox}(t_i), \epsilon_{oy}(t_i) \sim \mathcal{N}(0, \sigma_o^2), \quad (31)$$

where σ_o^2 is the variance of the obstacle detection noise.

H. Process Overview and Problem Formulation

The overall process of the obstacle avoidance task is described as follows. At the beginning of the task, the BS is assumed to have prior knowledge of the UAV's real initial position $\mathbf{p}(t_0)$ and its real destination position \mathbf{p}_{dst} . During subsequent time slots, the BS determines whether to transmit sensing and/or C&C signals based on the detected UAV position $\hat{\mathbf{p}}(t_i)$ and its associated detection variances $[\sigma_x^2(t_i), \sigma_y^2(t_i)]^\top$, as well as the detected positions of dynamic obstacles $\hat{\mathbf{p}}_o(t_i)$ and their corresponding variances $[\sigma_o^2, \sigma_o^2]^\top$, where $o \in \hat{\mathcal{O}}(t_i)$. For ease of understanding, suppose the BS transmits a sensing signal at the t_i -th time slot, from which the UAV's detected position $\hat{\mathbf{p}}(t_i)$ and the detection variance $[\sigma_x^2(t_i), \sigma_y^2(t_i)]^\top$ can be obtained. Let us assume there are dynamic obstacles around the UAV at t_i , and their detected positions and variances are $\hat{\mathbf{p}}_o(t_i)$ and $[\sigma_o^2, \sigma_o^2]^\top$, respectively. Based on the detected positions and variances of the UAV and obstacles, the BS decides whether to transmit a C&C signal and a new sensing signal at the next time slot t_{i+1} . This process is iteratively executed until the UAV successfully completes its task.

Our objectives are twofold: 1) to enable the UAV to complete the task as quickly as possible, and 2) to reduce the number of transmitted sensing and C&C signals. Therefore, the objective function is denoted as

$$\mathcal{P}1.1: \min_{\substack{\delta_c(t_i), \delta_s(t_i) \\ V(t_i), \phi(t_i)}} t_I \quad (32)$$

$$\text{s. t. } \|\mathbf{p}(t_i) - \mathbf{p}_o(t_i)\| > D_{\text{safe}}, \quad \forall t_i, o, \quad (32a)$$

$$\|\mathbf{p}(t_I) - \mathbf{p}_{\text{dst}}\| \leq D_{\text{thr}}, \quad (32b)$$

$$\mathcal{P}1.2: \min_{\substack{\delta_c(t_i), \delta_s(t_i) \\ V(t_i), \phi(t_i)}} \sum_{i=0}^I (\delta_c(t_i) + \delta_s(t_i)) \quad (33)$$

$$\text{s. t. } (32a), (32b),$$

where t_I in (32) denotes the time slot index for the UAV to reach its destination, $\sum_{i=0}^I (\delta_c(t_i) + \delta_s(t_i))$ in (33) represents the total number of transmitted sensing and C&C signals within t_I , D_{safe} is the safety distance for the UAV to avoid collision, D_{thr} is the threshold distance for UAV to reach its destination.

III. TRADITIONAL FRAMEWORK

In traditional research, obstacle avoidance and ISAC signal transmission have been studied as separate disciplines. Obstacle avoidance is primarily explored in the field of mobile robotics, whereas ISAC signal transmission is investigated in wireless communications. In existing ISAC research, sensing and communication signals are typically directed towards different targets, and both signals are transmitted continuously [12]. Robotic obstacle avoidance research commonly employs the dynamic window approach (DWA) [28] in highly dynamic environments, which can guide the robot to avoid dynamic obstacles while moving towards its destination. The basic principle of DWA is to sample the robot's linear and angular velocities within a feasible range constrained by its kinematics. Each velocity pair is evaluated using a cost function that accounts for distances to obstacles and the destination, and the optimal pair with the minimum cost is then selected. However, the DWA relies on the Euclidean norm to calculate distances, which leads to potential collisions in the presence of position detection errors. A typical solution is to introduce an inflation radius around the obstacle to account for such uncertainties [29]. As a result, the distance is calculated using both the Euclidean norm and the inflation radius.

Fig. 2 illustrates an example of the signal transmission under the traditional obstacle avoidance method. Specifically, at the beginning of the t_i -th time slot, the BS transmits an ISAC signal to the UAV, in which the C&C values are generated by the inflation based-DWA (I-DWA) using the detection positions of UAV and obstacles together with their variances at the t_{i-1} -th time slot. The sensing signal is reflected by the UAV and received by the BS. The C&C signal is received by the UAV, and then the UAV updates its motion state and moves at speed $V(t_i)$ and heading angle $\phi(t_i)$.

It is worth noting that, to ensure the safe operation of robotic systems, C&C signals are typically transmitted at very high frequencies [15]. Since C&C signals strongly depend on the sensed positions, the ISAC signals in our considered task must also be transmitted at such high frequencies, resulting in a large number of redundant C&C transmissions. For example,

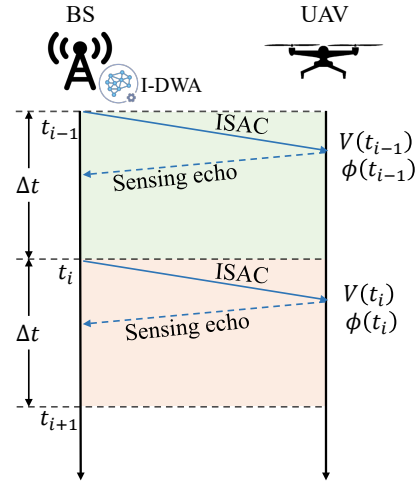


Fig. 2: Traditional signal transmission framework.

when there are no obstacles around the UAV, the BS may not need to transmit new sensing or C&C signals, and the UAV can continue executing the previously received C&C signal for several time slots despite random environmental influence. This motivates the development of a more efficient strategy that transmits sensing and/or C&C signals only when they are significantly beneficial to the goal of the task.

IV. GOSC FRAMEWORK

In this section, we present our proposed GOSC framework for ISAC-enabled robotic obstacle avoidance task. The framework comprises three main components that constitute a closed loop for sensing, C&C generation, and transmission for each time slot: a Kalman filter (KF) to mitigate the dependence of UAV position estimation on sensing signal transmissions, a Mahalanobis distance-based dynamic window approach (MD-DWA) to generate accurate C&C signals under uncertainty, and an effectiveness-aware deep Q-network (E-DQN) to ensure that sensing and C&C signals are transmitted only when they provide sufficient benefit to the task. These three components are introduced in detail in the subsequent subsections, followed by an overall description of the signal transmission process within the GOSC framework. For ease of distinction, the UAV's position detected from the sensing signal is denoted by $\hat{\mathbf{p}}$, the predicted position by the KF is denoted as $\hat{\mathbf{p}}$, and the final estimation position output from the KF is represented as $\tilde{\mathbf{p}}$.

A. Kalman Filter

We propose a KF that consists of two main functions: 1) predicting the position of the UAV at every time slot, and 2) reducing uncertainty of the sensing detected position. The first function provides a reference position for the UAV even when no signals are transmitted, such that the BS does not need to transmit sensing signals all the time. While the second function refines the detected position to achieve higher accuracy. To begin, we introduce the process transition model of the KF

$$\dot{\mathbf{p}}(t_i) = \dot{\mathbf{p}}(t_{i-1}) + \mathbf{D}\mathbf{v}(t_{i-1}) + \gamma(t_i), \quad (34)$$

$\mathbf{v}(t_{i-1}) = [V(t_{i-1}) \cos(\phi(t_{i-1})), V(t_{i-1}) \sin(\phi(t_{i-1}))]^\top$ represents the velocity along 2D Cartesian coordinate axes at the t_{i-1} -th time slot, $\mathbf{D} \in \mathbb{R}^{2 \times 2}$ is a matrix indicating the duration of speed $\mathbf{v}(t_{i-1})$, since the BS does not measure the transmission latency $\tau_c(t_{i-1})$ and C&C signals are not transmitted at some time slots, we suppose $\mathbf{D} = \mathbf{I}_2 \Delta t$, $\boldsymbol{\gamma} = [\eta_x(t_i), \eta_y(t_i)]^\top$ is the process noise. By (34), the KF can predict the UAV's position at every time slot. Specifically, the predicted position of the UAV at t_i can be denoted as

$$\dot{\mathbf{p}}(t_i) = \dot{\mathbf{p}}(t_{i-1}) + \mathbf{D}\mathbf{v}(t_{i-1}). \quad (35)$$

The covariance matrix $\hat{\mathbf{\Gamma}}(t_i) \in \mathbb{R}^{2 \times 2}$ of the predicted position $\dot{\mathbf{p}}(t_i)$ is represented as

$$\hat{\mathbf{\Gamma}}(t_i) = \hat{\mathbf{\Gamma}}(t_{i-1}) + \mathbf{Q}, \quad (36)$$

where $\hat{\mathbf{\Gamma}}(t_0) = \mathbf{0}_2$ is the initial position of the UAV that is known at the BS, $\mathbf{Q} = \mathbf{I}_2 \sigma_\eta^2$ is the covariance matrix of process noise. It can be found that although we can obtain a prediction position of the UAV at every time slot, the accumulated error increases if no sensing signals are transmitted over time, which in turn degrades the reliability of obstacle avoidance and may lead to collision. If the BS decides to transmit a sensing signal at the t_i -th time slot, according to equation (14), the sensing position is represented as $\hat{\mathbf{p}}(t_i) = \mathbf{p}(t_i) + [\epsilon_x(t_i), \epsilon_y(t_i)]^\top$. By combining the prediction and sensing uncertainties, the Kalman gain is obtained as

$$\mathbf{G}(t_i) = \hat{\mathbf{\Gamma}}^\top(t_i) [\hat{\mathbf{\Gamma}}(t_i) + \hat{\mathbf{\Gamma}}(t_i)]^{-1}, \quad (37)$$

where $\hat{\mathbf{\Gamma}}(t_i) \in \mathbb{R}^{2 \times 2}$ is the covariance matrix of $\hat{\mathbf{p}}(t_i)$ and is denoted as

$$\hat{\mathbf{\Gamma}}(t_i) = \begin{bmatrix} \sigma_x^2(t_i) & 0 \\ 0 & \sigma_y^2(t_i) \end{bmatrix}. \quad (38)$$

The Kalman gain $\mathbf{G}(t_i)$ serves as a weighting factor to balance the prediction position $\dot{\mathbf{p}}(t_i)$ and the sensing estimation position $\hat{\mathbf{p}}(t_i)$. Such that the KF can provide a more accurate position estimation and reduce the overall estimation uncertainty. The refined estimation position and its covariance matrix are given by

$$\begin{cases} \tilde{\mathbf{p}}(t_i) = \dot{\mathbf{p}}(t_i) + \mathbf{G}(t_i)(\hat{\mathbf{p}}(t_i) - \dot{\mathbf{p}}(t_i)), \\ \tilde{\mathbf{\Gamma}}(t_i) = (\mathbf{I}_2 - \mathbf{G}(t_i))\hat{\mathbf{\Gamma}}(t_i). \end{cases} \quad (39)$$

To enhance clarity, the workflow of the proposed KF is presented as follows: If no sensing signal is transmitted at t_i , the KF outputs $\tilde{\mathbf{p}}(t_i) = \dot{\mathbf{p}}(t_i)$ along with the covariance matrix $\tilde{\mathbf{\Gamma}}(t_i) = \hat{\mathbf{\Gamma}}(t_i)$, which together serves as the estimated information of the UAV. If a sensing signal is transmitted at t_i , the KF provides the refined position $\tilde{\mathbf{p}}(t_i)$ and the covariance matrix $\tilde{\mathbf{\Gamma}}(t_i)$ according to (39). At the same time, the prediction covariance matrix $\hat{\mathbf{\Gamma}}(t_i)$ is updated as $\tilde{\mathbf{\Gamma}}(t_i)$. If a C&C signal is transmitted at t_{i+1} , the velocity vector $\mathbf{v}(t_{i-1})$ in (34) is updated according to equation (22).

B. Mahalanobis Distance-based DWA

Based on $\tilde{\mathbf{p}}(t_i)$ and $\tilde{\mathbf{\Gamma}}(t_i)$, as well as the detected obstacle positions $\hat{\mathbf{p}}_o(t_i)$ and their corresponding variances $[\sigma_o^2, \sigma_o^2]^\top$, the BS generates C&C signals to guide the UAV avoiding

obstacles while moving towards its destination. Traditional inflation-based C&C methods are overly conservative: they ignore the directional characteristics of uncertainty and often overestimate obstacle regions, which reduces navigation efficiency. To overcome these limitations, we design a MD-DWA method to generate C&C signals. Specifically, the Mahalanobis distance [30] between the UAV and the detected obstacle $o \in \hat{\mathcal{O}}(t_i)$ is defined as

$$\begin{aligned} d_o^M &= \|\tilde{\mathbf{p}} - \mathbf{p}_o\|_M \\ &= \sqrt{(\tilde{\mathbf{p}} - \mathbf{p}_o)^\top (\tilde{\mathbf{\Gamma}} + \Phi_o)^{-1} (\tilde{\mathbf{p}} - \mathbf{p}_o)}, \end{aligned} \quad (40)$$

where the time slot index is t_i and is omitted due to space limitation, $\Phi_o = \mathbf{I}_2 \sigma_o^2$ is the covariance matrix of the o -th detected obstacle. The detailed generation process of C&C signals based on the MD-DWA method is described as follows. Suppose the BS transmits a sensing signal at t_i , after receiving the sensing echo signal, the BS generates a feasible movement velocity and forward angle set. According to equation (23), the feasible set can be denoted as

$$\begin{aligned} \Omega(t_i) &= \left\{ (\check{V}(t_i), \check{\phi}(t_i)) \mid \max\{0, V(t_{i-1}) - \Delta V\} \leq \check{V}(t_i) \leq \right. \\ &\quad \left. \min\{V(t_{i-1}) + \Delta V, V_{\max}\}, \max\{0, \phi(t_{i-1}) - \Delta\phi\} \right. \\ &\quad \left. \leq \check{\phi}(t_i) \leq \min\{\phi(t_{i-1}) + \Delta\phi, 2\pi\} \right\}. \end{aligned} \quad (41)$$

For each candidate pair $(\check{V}(t_i), \check{\phi}(t_i)) \in \Omega(t_i)$, a forward prediction trajectory $\Xi(t_i)$ is generated over the next I_p time slots using the KF prediction model (34), which can be expressed as the discrete sequence

$$\Xi(t_i) = \left\{ [\check{p}_x(t_{i+b}), \check{p}_y(t_{i+b})]^\top : b = 1, 2, \dots, I_p \right\}, \quad (42)$$

in which

$$\begin{bmatrix} \check{p}_x(t_{i+b}) \\ \check{p}_y(t_{i+b}) \end{bmatrix} = \begin{bmatrix} \tilde{p}_x(t_i) + \check{V}(t_i) \cos(\check{\phi}(t_i)) b \Delta t \\ \tilde{p}_y(t_i) + \check{V}(t_i) \sin(\check{\phi}(t_i)) b \Delta t \end{bmatrix}, \quad (43)$$

To evaluate collision risk along the predicted trajectory, the minimum Mahalanobis distance to the detected obstacles is calculated as

$$d_{\min}^M(\check{V}(t_i), \check{\phi}(t_i)) = \min_b \min_o d_o^M(t_{i+b}), \quad (44)$$

in which $\mathbf{p}_o(t_{i+b}) = \mathbf{p}_o(t_i)$ is constant over the horizon since obstacle motions are unknown and need to be detected by cooperative BSs, $\Phi_o(t_{i+b}) = \Phi_o(t_i) + b \Delta t \mathbf{I}_2$. Let b^* and o^* denote the prediction step and obstacle yielding this minimum Mahalanobis distance, respectively.

Lemma 2. *To avoid collision with obstacles, the minimum Mahalanobis distance must satisfy*

$$d_{\min}^M(\check{V}(t_i), \check{\phi}(t_i)) \geq \sqrt{\chi_{2,0.99}^2 + \frac{D_{\text{safe}}}{\lambda_{\min}(\boldsymbol{\Sigma}(t_i))}}, \quad (45)$$

where $\chi_{2,0.99}^2$ is the 99% confidence threshold of a chi-squared (χ^2) distribution with two degrees of freedom, $\boldsymbol{\Sigma}(t_i) = \Phi_{o^*}(t_i) + \hat{\mathbf{\Gamma}}(t_{i+b^*})$ is the covariance matrix of $d_{\min}^M(\check{V}(t_i), \check{\phi}(t_i))$, $\lambda_{\min}(\boldsymbol{\Sigma}(t_i))$ is the minimum eigenvalue of $\boldsymbol{\Sigma}(t_i)$.

Proof. Please see Appendix B. \square

The feasible candidate set is thus refined to $\Omega'(t_i)$, which only includes the candidate pair $(\check{V}(t_i), \check{\phi}(t_i))$ satisfying (45). For each $(\check{V}(t_i), \check{\phi}(t_i)) \in \Omega'(t_i)$, the Mahalanobis distance between the predicted trajectory endpoint $\check{\mathbf{p}}(t_{i+I_p})$ and the destination \mathbf{p}_{dst} is computed as

$$d_{\text{des}}^M(\check{V}(t_i), \check{\phi}(t_i)) = \sqrt{(\check{\mathbf{p}}(t_{i+I_p}) - \mathbf{p}_{\text{dst}})^\top (\tilde{\mathbf{\Gamma}}(t_{i+I_p}))^{-1} (\check{\mathbf{p}}(t_{i+I_p}) - \mathbf{p}_{\text{dst}})}. \quad (46)$$

To realize obstacle avoidance and destination approaching related to P1.1, an evaluation function is defined as

$$E(\check{V}(t_i), \check{\phi}(t_i)) = \frac{d_{\text{dst}}^M(\check{V}(t_i), \check{\phi}(t_i))}{d_{\text{dst}}^{M^*}} + \frac{d_{\text{min}}^{M^*}}{d_{\text{min}}^M(\check{V}(t_i), \check{\phi}(t_i))}, \quad (47)$$

where $d_{\text{dst}}^{M^*}$ and $d_{\text{min}}^{M^*}$ are the maximum and the minimum values of $d_{\text{dst}}^M(\check{V}(t_i), \check{\phi}(t_i))$ and $d_{\text{min}}^M(\check{V}(t_i), \check{\phi}(t_i))$, respectively. The optimal control pair is then selected as

$$(V(t_i), \phi(t_i)) = \arg \min_{(\check{V}(t_i), \check{\phi}(t_i)) \in \Omega'(t_i)} E(\check{V}(t_i), \check{\phi}(t_i)) \quad (48)$$

The overall procedure of the MD-DWA based C&C signal generation is summarized in **Algorithm 1**.

Algorithm 1 The MD-DWA based C&C Signal Generation

Input: Estimated UAV and obstacles positions with covariance matrices.

Output: The C&C velocity $V(t_i)$ and heading angle $\phi(t_i)$.

- 1: **while** the task is not completed **do**
 - 2: **if** a sensing signal is transmitted at t_{i-1} **then**
 - 3: Generate a feasible set $\Omega(t_i)$ via (41).
 - 4: **if** no obstacles are detected **then**
 - 5: Evaluate candidates in $\Omega(t_i)$ using (46).
 - 6: **else**
 - 7: Refine the feasible set as $\Omega'(t_i)$ via (45).
 - 8: Calculate the evaluation function according to (47).
 - 9: **end if**
 - 10: **end if**
 - 11: Select the optimal $V(t_i)$ and $\phi(t_i)$ based on (48).
 - 12: **end while**
-

C. Effectiveness-Aware DQN for Sensing and C&C Signal Transmission

Based on the KF and MD-DWA, we develop an E-DQN to control the transmission of sensing and C&C signals. To align with the objective functions in (32) and (33), the state, action, and reward in E-DQN are carefully designed. Specifically, the observation state of E-DQN at the t_i -th time slot is defined as

$$\mathcal{S}(t_i) \triangleq \left\{ d_{\text{dst}}^M(t_i), d_{\text{obs}}^M(t_i), \det(\tilde{\mathbf{\Gamma}}(t_i)), t_i, N_\delta(t_i) \right\}, \quad (49)$$

where $d_{\text{dst}}^M(t_i)$ is the Mahalanobis distance to the destination, $d_{\text{obs}}^M(t_i)$ is the minimum Mahalanobis distance to the detected obstacles, $\det(\tilde{\mathbf{\Gamma}}(t_i))$ is the determinant of $\tilde{\mathbf{\Gamma}}(t_i)$, $N_\delta(t_i) = \sum_i (\delta_c(t_i) + \delta_s(t_i))$ is the accumulated number of transmitted

signals up to t_i . The action of DQN at the t_i -th time slot is defined as

$$\mathcal{A}(t_i) = \{0, 1, 2\}, \quad (50)$$

where 0, 1, 2 represents stay silent, transmit sensing signal at t_i and do not transmit communication signal at t_{i+1} , transmit sensing signal at t_i and transmit communication signal at t_{i+1} , respectively. The reward of E-DQN at t_i is defined as

$$R(t_i) \triangleq \text{VoI}(t_i) - \text{Cost}(t_i) - \Psi_{\text{step}}(t_i) - \Psi_{\text{col}}(t_i), \quad (51)$$

where each term is specified below:

(a) $\text{VoI}(t_i)$ contains the VoI of sensing and communication signals, which is defined as

$$\text{VoI}(t_i) \triangleq \text{VoI}_s(t_i) + \text{VoI}_c(t_i), \quad (52)$$

in which the VoI of the sensing signal $\text{VoI}_s(t_i)$ is quantified by the reduction in estimation error entropy

$$\begin{aligned} \text{VoI}_s(t_i) &\triangleq \mathbb{H}(\tilde{\mathbf{\Gamma}}(t_{i-1})) - \mathbb{H}(\tilde{\mathbf{\Gamma}}(t_i)) \\ &= \frac{1}{2} \ln \left(\frac{\det(\tilde{\mathbf{\Gamma}}(t_{i-1}))}{\det(\tilde{\mathbf{\Gamma}}(t_i))} \right), \end{aligned} \quad (53)$$

where $\mathbb{H}(\tilde{\mathbf{\Gamma}}(t_i))$ denotes the entropy of the covariance matrix $\tilde{\mathbf{\Gamma}}(t_i)$. The VoI of the C&C signal $\text{VoI}_c(t_i)$ can be measured by navigation improvement of the UAV

$$\text{VoI}_c(t_i) \triangleq \Delta \|\mathbf{p}(t_i) - \mathbf{p}_{\text{dst}}\| + \Delta 1_{\text{col}}, \quad (54)$$

where $\Delta \|\mathbf{p}(t_i) - \mathbf{p}_{\text{dst}}\|$ is the difference in UAV–destination distance with and without transmitting the C&C signal. Note that although the real position is unobservable, the agent interacts with the environment based on its real position; thus, the reward is computed accordingly. $\Delta 1_{\text{col}} = 1$ if transmitting the C&C signal at t_i can help UAV avoid obstacle while no transmission causes collision, and 0 otherwise.

(b) $\text{Cost}(t_i)$ is the cost for transmitting sensing and C&C signals. Let us denote $A(t_i) \in \mathcal{A}(t_i)$, and $\text{Cost}(t_i)$ can be defined as

$$\text{Cost}(t_i) \triangleq \begin{cases} 0.5, & \text{if } A(t_i) = 1, \\ 1, & \text{if } A(t_i) = 2, \\ 0, & \text{otherwise.} \end{cases} \quad (55)$$

(c) $\Psi_{\text{step}}(t_i)$ is the step penalty introduced to encourage E-DQN to complete the task as quickly as possible. Its value increases gradually with t_i , thereby penalizing longer time. Specifically, it is defined as

$$\Psi_{\text{step}}(t_i) \triangleq \frac{1}{1 + e^{-0.1 \cdot i}}, \quad (56)$$

which adopts a sigmoid form to ensure smooth growth and bounded normalization.

(d) $\Psi_{\text{col}}(t_i)$ is the collision penalty introduced to avoid collision, which is given as

$$\Psi_{\text{col}}(t_i) \triangleq \begin{cases} \Psi, & \text{if } \|\mathbf{p}(t_i) - \mathbf{p}_o(t_i)\| \leq D_{\text{safe}}, \\ 0, & \text{otherwise.} \end{cases} \quad (57)$$

With the above definitions, the original problems $\mathcal{P}1.1$ and $\mathcal{P}1.2$ can be reformulated as the following Markov decision process (MDP) optimization problem

$$\mathcal{P}2: \max_{\pi_{\omega}(A(t_i)|\mathcal{S}(t_i))} \mathbb{E}_{\pi_{\omega}} \left[\sum_{i=0}^I \gamma^i R(t_i) \right] \quad (58)$$

where $\pi_{\omega}(A(t_i)|\mathcal{S}(t_i))$ denotes the E-DQN policy parameterized by ω , specifying which action $A(t_i) \in \mathcal{A}(t_i)$ is taken when observing state $\mathcal{S}(t_i)$, the scalar $\gamma \in (0, 1)$ is the discount factor. Following the classical DQN structure [31], two deep neural networks with identical architectures are maintained in E-DQN. One is called ‘eval network’ with parameters ω , used for learning and decision-making; the other is called ‘target network’, updated periodically to stabilize training. To obtain the optimal parameters, the E-DQN framework is trained in the following way: At each time slot t_i , the eval network observes the current state $\mathcal{S}(t_i)$ and selects an action $A(t_i)$ according to π_{ω} . To balance exploration and exploitation, the action is chosen via an ε -greedy strategy

$$A(t_i) \triangleq \begin{cases} \arg \max_{A(t_i) \in \mathcal{A}(t_i)} Q(\mathcal{S}(t_i), A(t_i)|\omega), & \text{if } \varepsilon \leq \varepsilon_0, \\ \text{a random action,} & \text{if } \varepsilon > \varepsilon_0, \end{cases} \quad (59)$$

where $\varepsilon \in [0, 1]$ is a random variable, $\varepsilon_0 \in [0, 1]$ is the exploration probability threshold. $Q(\mathcal{S}(t_i), A(t_i)|\omega)$ is the state-action value function [32] and defined as

$$Q(\mathcal{S}(t_i), A(t_i)|\omega) \triangleq \mathbb{E}_{\pi_{\omega}} \left[\sum_{\varsigma=0}^{I-i} \gamma^{\varsigma} R(t_{i+\varsigma}) \middle| \mathcal{S}(t_i), A(t_i) \right]. \quad (60)$$

After executing action $A(t_i)$, the agent receives reward $R(t_i)$ and the environment transitions to next state $\mathcal{S}(t_{i+1})$. The agent stores the tuple $(\mathcal{S}(t_i), A(t_i), R(t_i), \mathcal{S}(t_{i+1}))$ as an experience into its memory buffer. When the memory buffer is full, the DQN is trained by randomly sampling N_0 experiences

$$(\mathcal{S}_n, A_n, R_n, \mathcal{S}'_n), \quad n = 1, 2, \dots, N_0, \quad (61)$$

which helps break the temporal correlation among experiences. Based on these random samples, E-DQN minimizes the mean squared error between the predicted and the target state-action values, which is calculated as

$$L(\omega) = \frac{1}{N_0} \sum_{n=1}^{N_0} \left[R_n + \gamma \max_{A'_n} Q(\mathcal{S}'_n, A'_n | \omega^-) - Q(\mathcal{S}_n, A_n | \omega) \right]^2. \quad (62)$$

where ω^- denotes the parameters of target network. The eval network parameters ω are updated via gradient descent

$$\omega \leftarrow \omega + L_r \nabla_{\omega} L(\omega), \quad (63)$$

where $L_r \in (0, 1)$ is the learning rate of the eval network. To stabilize learning, the target network parameters are updated every N_U steps

$$\omega^- \leftarrow \omega. \quad (64)$$

The overall training procedure is summarized in **Algorithm 2**.

Algorithm 2 E-DQN for Signal Transmission

Input: Observation $\mathcal{S}(t_i)$ at each time slot

Output: Action $A(t_i)$ at each time slot.

- 1: Initialize eval network parameters ω and target network parameters $\omega^- \leftarrow \omega$.
 - 2: Set memory buffer capacity C_M . Initialize counter $c \leftarrow 0$.
 - 3: Collect initial experiences until the memory buffer is full.
 - 4: **for** each episode **do**
 - 5: **while** the task is not completed **do**
 - 6: Select action $A(t_i)$ based on state $\mathcal{S}(t_i)$ using the ε -greedy policy in (59).
 - 7: Execute action $A(t_i)$. The environment transitions into next state $\mathcal{S}(t_{i+1})$ and the agent receives reward $R(t_i)$.
 - 8: Store experience tuple $(\mathcal{S}(t_i), A(t_i), R(t_i), \mathcal{S}(t_{i+1}))$ in the memory buffer at index $c \bmod C_M$.
 - 9: Randomly sample N_0 experiences from the memory buffer.
 - 10: Compute the loss $L(\omega)$ using (62) and update eval-network parameters via (63).
 - 11: **if** $c \bmod N_U = 0$ **then**
 - 12: Update target network parameters: $\omega^- \leftarrow \omega$.
 - 13: **end if**
 - 14: Update state $\mathcal{S}(t_i) \leftarrow \mathcal{S}(t_{i+1})$ and counter $c \leftarrow c+1$.
 - 15: **end while**
 - 16: **end for**
-

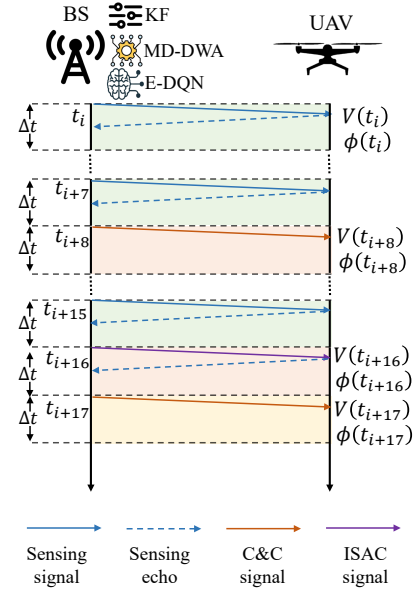


Fig. 3: An example of sensing and C&C signal transmission process under our proposed GOSC framework.

D. Sensing and C&C Signal Transmission Process

For better understanding, Fig. 3 illustrates an example of the sensing and C&C signal transmission process of our proposed GOSC framework. Specifically, at the beginning of the t_i -th time slot, E-DQN observes the environment state $\mathcal{S}(t_i)$ and decides to transmit only a sensing signal, i.e. $A(t_i) = 1$. During the subsequent six time slots, the BS remains silent, i.e., $A(t_{i+(1\sim6)}) = 0$. At t_{i+7} , the E-DQN chooses to transmit

a sensing signal at the current slot and a C&C signal at the next slot t_{i+8} , i.e., $A(t_{i+7}) = 2$, followed by another seven idle slots. At t_{i+15} and t_{i+16} , the E-DQN again selects $A(t) = 2$. It can be observed that, unlike the traditional framework where ISAC signals are transmitted continuously, the BS in our GOSC framework selectively transmits sensing, C&C, or ISAC signals. Consequently, the overall communication overhead can be significantly reduced.

V. SIMULATIONS AND ANALYSIS

In this section, extensive simulations are conducted to evaluate the performance of our proposed GOSC framework. The key simulation parameters are summarized as follows. The time slot interval is set to $\Delta t = 5$ ms. The UAV starts from the initial position $\mathbf{p}(t_0) = [0.1, 0.1]^T$ m and flies toward the destination $\mathbf{p}_{\text{dst}} = [10, 10]^T$ m, maintaining a fixed altitude of $H = 10$ m. The radar cross section of the UAV is $\sigma_{\text{RCS}} = 0.1$ m². The UAV's maximum speed is $V_{\text{max}} = 4$ m/s, and the maximum changes in heading angle and speed per time slot are $\Delta\phi = \pi/6$ rad and $\Delta V = 0.5$ m/s, respectively. The variance of the environmental disturbance affecting the UAV's motion is $\sigma_{\eta}^2 = 0.005$. The safety distance to avoid collision is $D_{\text{safe}} = 0.5$ m, while the threshold distance for the UAV to reach its destination is $D_{\text{thr}} = 0.3$ m. A total of $N_o = 10$ dynamic obstacles are randomly distributed within a square area of $[2, 8] \times [2, 8]$ m² along the UAV's flight route. Each obstacle moves with horizontal velocity components $V_{ox}(t_i)$ and $V_{oy}(t_i)$ uniformly distributed within $[-1, 1]$ m/s. The detection noise for each obstacle has variance $\sigma_o^2 = 0.001$. The scanning radius for obstacles is $R_{\text{scan}} = 0.4$ m. The BS is located at $\mathbf{p}_{\text{BS}} = [0, 0]^T$ m on the ground. It is equipped with $K = 128$ antennas and transmits ISAC signals over $M = 2500$ subcarriers, with a subcarrier spacing of $\Delta f = 120$ kHz. The carrier frequency is $f_c = 60$ GHz, and the antenna element spacing is $D = 2.5$ mm. The transmit power of the BS is $P = 20$ dBm, while the power spectral density of the AWGN is $\sigma_0^2 = -174$ dBm/Hz. The Rician factor of the wireless channel is set to $\kappa = 8$ dB. Each C&C signal has a size of $S = 1$ kbit and is mapped $L = 50$ times across subcarriers for reliable transmission. The discrete angular grid for beamforming contains $N_{\theta} = 500$ points. The confidence level factor is $B = 2.576$, corresponding to a 99% confidence level. The prediction horizon in MD-DWA is set to $I_p = 20$ time slots. The parameters of DQN are summarized in **Table I**.

TABLE I: DQN Parameter Settings

Parameter description	Value
Collision penalty Ψ	10
Discount factor γ	0.9
Exploration probability threshold ε	0.8
Memory buffer capacity C_M	8000
Sample batch N_0	32
Learning rate L_R	0.001
Target network update step N_U	100
Number of hidden layers	2
Number of neurons in each hidden layer	128

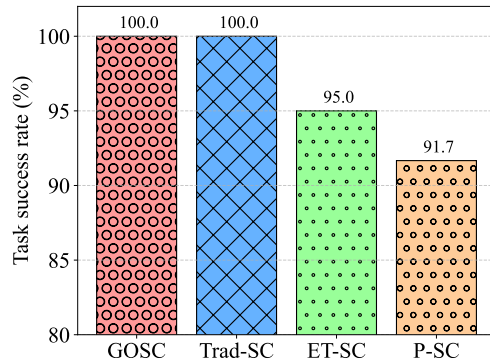


Fig. 4: Task success rate.

For comparison, we present the other three schemes as baselines:

- **Traditional sensing and communication signals transmission (Trad-SC)** [12]. As discussed in Section III, ISAC signals are transmitted at each time slot. The inflation-based DWA is employed to generate C&C signals.
- **Periodic sensing and communication signal transmission (P-SC)** [33]. The sensing and C&C signals are transmitted every 10 time slots. The KF and MD-DWA are used for prediction and C&C signal generation.
- **Event-trigger sensing and communication signal transmission (ET-SC)** [34]. This is a commonly method in robotic control system, in which control signals are triggered when the accumulated error exceeds a threshold. We extend the method for sensing and C&C signals transmission: If no obstacles are detected, signals are transmitted when $\mathbb{H}(\tilde{\mathbf{T}}(t_i)) \geq 0.01$; otherwise, they are transmitted when $\mathbb{H}(\tilde{\mathbf{T}}(t_i)) \geq 0.001$. The KF and MD-DWA are also adopted in this scheme.

We conduct simulations over 60 random seeds, where the initial obstacle positions vary across seeds, and all the following simulation results are average values. First, the task success rates under different schemes are shown in Fig. 4, representing the probability that the UAV successfully avoids obstacles and reaches its destination. It is no surprising that Trad-SC achieves a 100% success rate, as ISAC signals are transmitted every time slot. This enables the BS to continuously update the UAV's position and provide real-time control. Remarkably, our proposed GOSC also achieves a 100% success rate. This can be attributed to the effectiveness-aware DQN, which selectively transmits task-critical signals based on their effectiveness level. In contrast, ET-SC achieves a 95% success rate. Indeed, its performance is highly sensitive to the signal transmission threshold. A lower threshold increases the likelihood of success but requires the BS to transmit more signals. Finally, P-SC yields the lowest success rate. The main reason is that when the UAV approaches obstacles, essential C&C signals are needed to guide avoidance maneuvers. However, under P-SC, signal transmission follows a fixed periodic schedule, which may fail to provide vital updates when the UAV is approaching obstacles.

To further examine objective-related performance, Fig. 5

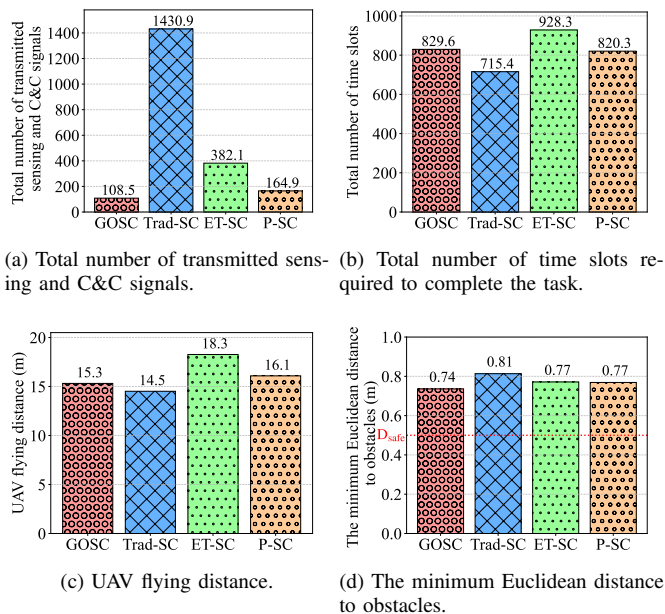


Fig. 5: Performances under different schemes.

presents the total number of transmitted signals, total number of time slots to complete the task, UAV flying distance, and the minimum Euclidean distance to obstacles under the four schemes, where only successful tasks are considered for fair comparison. As shown in Fig. 5a, GOSC transmits the fewest signals, reducing the number of transmissions by 92.4% compared to Trad-SC. This advantage stems from the GOSC framework, which can continuously predict the position of UAV and transmit only those effectiveness-relevant signals for safe navigation, thereby eliminating redundant signal transmission. ET-SC and P-SC also reduce the number of transmissions, but this comes at the expense of degraded reliability. Interestingly, when combined with the success rate results of Trad-SC, ET-SC and P-SC in Fig. 4, it can be found that bit-oriented schemes face a distinct tradeoff where higher reliability demands more transmissions, GOSC effectively breaks this limitation, achieving high reliability and low communication costs simultaneously.

Fig. 5b and Fig. 5c present the total number of time slots for the UAV to complete the task and the corresponding flying path length, respectively. Trad-SC achieves the fewest time slots and the shortest flying distance, owing to continuous signal transmission that ensures real-time trajectory update. The flying path length of GOSC is shorter than that of P-SC, while the average task completion time of GOSC is comparable to P-SC. This is because GOSC selectively transmits signals: while the content of C&C signals remains effective, they are not transmitted every time after sensing to balance transmission cost and task completion time, which may prolong the overall task duration. ET-SC exhibits the worst performance in both metrics. This is due to its threshold-triggered signal transmission, where critical updates may be postponed if the threshold condition is not met, causing inefficient avoidance maneuvers and consequently longer path and completion time. From Fig. 5d, we observe that the average minimum Euclidean distance of Trad-SC is larger than that of

the other three schemes. This is because the inflation-based DWA typically overestimates the obstacle space, resulting in more conservative avoidance maneuvers. In contrast, the MD-DWA provides a more accurate characterization of UAV and obstacles uncertainty, allowing the UAV to maintain a shorter but still safe distance from obstacles.

To gain deeper insight into signal transmission under the four schemes, Fig. 6 depicts the detailed transmission statistics for successful tasks. As shown in Fig. 6a and Fig. 6b, the sensing and communication functions are coupled in bit-oriented transmission schemes Trad-SC, ET-SC and P-SC. In contrast, GOSC sometimes omits the transmission of C&C signals after sending sensing signals. This is reasonable, as prolonged transmission of sensing signals leads to increasing uncertainty. Consequently, it becomes necessary for the BS to transmit sensing signals. But sometimes, the UAV's actual movement speed and heading angle are aligned with expectations, in which case there is no need to transmit C&C signals at subsequent time slots. Fig. 6c shows the total number of transmission slots, which represents the time slots during which sensing and/or communication signals are transmitted. This metric reflects the wireless resource allocation cost. It is seen that GOSC reduces the average number of transmission slots by 85.5% compared with Trad-SC, highlighting its strong capability in saving scarce wireless resources.

To provide an intuitive understanding of UAV movement in the task, we select a representative random seed and illustrate the UAV trajectories under the four schemes in Fig. 7. For clarity, the obstacle detection process is omitted, as it is difficult to visualize in a static figure. We use varying color lines to represent the UAV trajectories over time. The black lines represent the movement of obstacles. Overall, the UAV trajectories appear broadly consistent across the four schemes, since all adopt the DWA algorithm. However, noticeable long linear trajectory can be observed in GOSC. This occurs because the BS does not transmit new C&C signals and the UAV repeatedly executes the previously received C&C signals. In such scenarios, no collision risk arises, as there are no obstacles directly ahead of the UAV. Conversely, when the UAV enters regions with a high density of obstacles, the straight linear trajectory becomes shorter. This is because vital C&C signals must be transmitted to avoid collision.

VI. CONCLUSIONS

This paper investigated an integrated sensing and communication (ISAC)-enabled BS for the unmanned aerial vehicle (UAV) obstacle avoidance task, and proposed a goal-oriented semantic communication (GOSC) framework to efficiently transmit sensing and command-and-control (C&C) signals. By integrating a Kalman filter (KF), a Mahalanobis distance-based dynamic window approach (MD-DWA), and an effectiveness-aware deep Q-network (E-DQN), the framework can efficiently transmit sensing and C&C signals at times when the transmission can benefit for the effectiveness of the robotic task. Specifically, the KF effectively reduces redundant sensing signal transmissions while improving UAV position estimation through sensing-prediction fusion. The MD-DWA

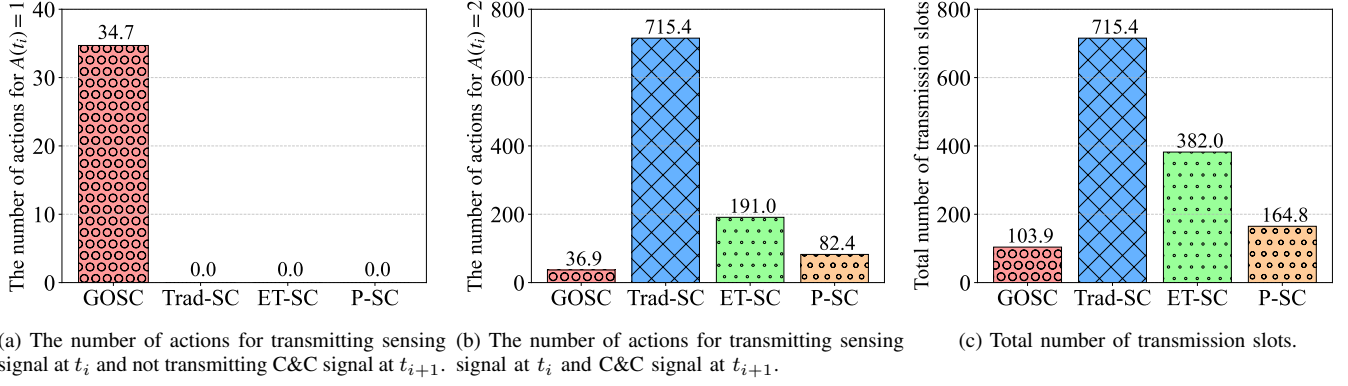


Fig. 6: The number of transmitted sensing and C&C signals, and their total transmission time slots.

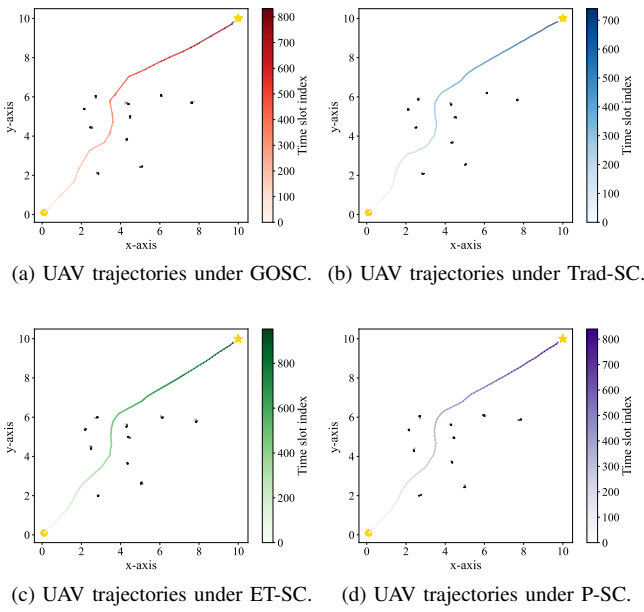


Fig. 7: UAV trajectories under different schemes.

generates precise and collision-free C&C signals by leveraging a mathematically derived minimum Mahalanobis distance. The E-DQN further enhances communication efficiency by transmitting signals only when their value of information (VoI) is significant. Extensive simulations demonstrate that, compared to the traditional continuous ISAC transmission framework, our proposed GOSC framework can achieve the same 100% task success rate while reducing the number of transmitted sensing and C&C signals by 92.4% and the required transmission time slots by 85.5%.

APPENDIX A PROOF OF LEMMA 1

For easy description, we omit the index of time slot t_i . Define a conversion function from polar coordinate to Cartesian coordinate as

$$\mathbf{f}(r, \theta) = \begin{bmatrix} x(r, \theta) \\ y(r, \theta) \end{bmatrix} = \begin{bmatrix} r \cos(\theta) \\ r \sin(\theta) \end{bmatrix}. \quad (65)$$

We approximate $\mathbf{f}(r, \theta)$ by a first-order Taylor expansion around the nominal values $(\hat{r}, \hat{\theta})$, which can be represented as

$$\mathbf{f}(r, \theta) \approx \mathbf{f}(\hat{r}, \hat{\theta}) + \mathbf{J}(\hat{r}, \hat{\theta}) \begin{bmatrix} r - \hat{r} \\ \theta - \hat{\theta} \end{bmatrix}, \quad (66)$$

in which $\mathbf{J}(\hat{r}, \hat{\theta})$ is the Jacobian matrix that obtains the first-order partial derivatives of the function $\mathbf{f}(r, \theta)$ at $(\hat{r}, \hat{\theta})$, which can be written as

$$\mathbf{J}(\hat{r}, \hat{\theta}) = \left. \frac{\partial(x, y)}{\partial(r, \theta)} \right|_{(\hat{r}, \hat{\theta})} = \begin{bmatrix} \cos(\hat{\theta}) & -\hat{r} \sin(\hat{\theta}) \\ \sin(\hat{\theta}) & \hat{r} \cos(\hat{\theta}) \end{bmatrix}. \quad (67)$$

After resorting (66), we can obtain

$$\begin{bmatrix} \epsilon_x \\ \epsilon_y \end{bmatrix} \approx \mathbf{J}(\hat{r}, \hat{\theta}) \begin{bmatrix} \epsilon_r \\ \epsilon_\theta \end{bmatrix}. \quad (68)$$

APPENDIX B PROOF OF LEMMA 2

Let \mathbf{z} denote the relative position between the UAV and the obstacle at the minimum Mahalanobis distance, we have $\mathbf{z} \sim \mathcal{N}(\boldsymbol{\mu}, \boldsymbol{\Sigma})$, in which

$$\boldsymbol{\mu} = \begin{bmatrix} \check{p}_x(t_{i+a^*}) - p_{o^*x} \\ \check{p}_y(t_{i+a^*}) - p_{o^*y} \end{bmatrix}, \quad \boldsymbol{\Sigma} = \mathring{\Gamma}(t_{i+a^*}) + \Phi_{o^*}(t_i). \quad (69)$$

According to equation (7) in [35], the squared Mahalanobis distance $\|\mathbf{z} - \boldsymbol{\mu}\|_M^2 = (\mathbf{z} - \boldsymbol{\mu})^\top \boldsymbol{\Sigma}^{-1} (\mathbf{z} - \boldsymbol{\mu})$ follows a chi-squared (χ^2) distribution with degrees of freedom equal to the dimension of \mathbf{z} , i.e., $(\mathbf{z} - \boldsymbol{\mu}) \sim \chi_2^2$. For a tolerated collision probability ϱ , define the confidence threshold $\varpi = \chi_{2, 1-\varrho}^2$. The corresponding $(1 - \varrho)$ -confidence ellipse is given as

$$\mathcal{E}_\varpi = \{\mathbf{e} \in \mathbb{R}^{2 \times 1} : \mathbf{e}^\top \boldsymbol{\Sigma}^{-1} \mathbf{e} \leq \varpi\}, \quad (70)$$

where $\mathbf{e} = \mathbf{z} - \boldsymbol{\mu}$ has zero mean. The UAV also has a hard safety distance D_{safe} . After accounting for this distance, if the confidence ellipse does not contain the origin point, we can determine that the UAV can avoid collision with probability at least $(1 - \varrho)$. The condition can be written as

$$\mathbf{0} \notin \boldsymbol{\mu} + \mathcal{E}_\varpi \oplus \mathcal{D}, \quad (71)$$

where $\mathcal{D} = \{\mathbf{u} : \|\mathbf{u}\| \leq D_{\text{safe}}\}$ and \oplus denotes the Minkowski sum. Equivalently, (71) can be transformed as

$$\min_{\mathbf{e} \in \mathcal{E}_\varpi, \|\mathbf{u}\| \leq D_{\text{safe}}} \|\boldsymbol{\mu} + \mathbf{e} + \mathbf{u}\|_M > 0. \quad (72)$$

By the triangle inequality, we have

$$\min_{e \in \mathcal{E}_\omega, \|u\| \leq D_{\text{safe}}} \|\mu + e + u\|_M \geq \|\mu\|_M - \sup_{e \in \mathcal{E}_\omega} \|e\|_M - \sup_{\|u\|_2 \leq D_{\text{safe}}} \|u\|_M, \quad (73)$$

where $\sup(\cdot)$ denotes the least upper bound of a set. By definition of \mathcal{E}_ω , we have $\sup_{e \in \mathcal{E}_\omega} \|e\|_M = \sqrt{\omega}$. To bound $\sup_{\|u\|_2 \leq D_{\text{safe}}} \|u\|_M$, we use the Rayleigh quotient inequality [36], which can be written as

$$u^\top \Sigma^{-1} u = \frac{u^\top \Sigma^{-1} u}{u^\top u} u^\top u \leq \lambda_{\max}(\Sigma^{-1}) \|u\|^2 = \frac{\|u\|^2}{\lambda_{\min}(\Sigma)}, \quad (74)$$

since Σ is symmetric positive definite, its smallest eigenvalue satisfies $\lambda_{\min}(\Sigma) > 0$. Taking square roots gives

$$\|u\|_M \leq \frac{\|u\|}{\sqrt{\lambda_{\min}(\Sigma)}}. \quad (75)$$

Hence

$$\sup_{\|u\|_2 \leq D_{\text{safe}}} \|u\|_M \leq \frac{D_{\text{safe}}}{\sqrt{\lambda_{\min}(\Sigma)}}. \quad (76)$$

Therefore, a sufficient deterministic condition for (72) to hold is

$$\|\mu\|_M > \sqrt{\omega} + \frac{D_{\text{safe}}}{\sqrt{\lambda_{\min}(\Sigma)}}. \quad (77)$$

REFERENCES

- [1] A. Pandey, S. Pandey, and D. Parhi, "Mobile robot navigation and obstacle avoidance techniques: A review," *Int. Robot. Autom. J.*, vol. 2, no. 3, pp. 1–12, May 2017.
- [2] J. Lv, C. Qu, S. Du, X. Zhao, P. Yin, N. Zhao, and S. Qu, "Research on obstacle avoidance algorithm for unmanned ground vehicle based on multi-sensor information fusion," *Math. Biosci. Eng.*, vol. 18, no. 2, pp. 1022–1039, 2021.
- [3] A. N. A. Rafai, N. Adzhar, and N. I. Jaini, "A review on path planning and obstacle avoidance algorithms for autonomous mobile robots," *J. Robot.*, vol. 2022, no. 1, pp. 1–14, Dec. 2022.
- [4] X. Liu, S. Wen, Z. Jiang, W. Tian, T. Z. Qiu, and K. M. Othman, "A multisensor fusion with automatic vision–lidar calibration based on factor graph joint optimization for slam," *IEEE Trans. Instrum. Meas.*, vol. 72, pp. 1–9, Oct. 2023.
- [5] P. Chen, J. Pei, W. Lu, and M. Li, "A deep reinforcement learning based method for real-time path planning and dynamic obstacle avoidance," *Neurocomputing*, vol. 497, pp. 64–75, Aug. 2022.
- [6] F. Liu, Y. Cui, C. Masouros, J. Xu, T. X. Han, Y. C. Eldar, and S. Buzzi, "Integrated sensing and communications: Toward dual-functional wireless networks for 6g and beyond," *IEEE J. Sel. Areas Commun.*, vol. 40, no. 6, pp. 1728–1767, Jun. 2022.
- [7] J. Liu, C. Zhou, M. Sheng, H. Yang, X. Huang, and J. Li, "Resource allocation for adaptive beam alignment in uav-assisted integrated sensing and communication networks," *IEEE J. Sel. Areas Commun.*, vol. 43, no. 1, pp. 350–363, Jan. 2025.
- [8] C. Dou, N. Huang, Y. Wu, L. Qian, and T. Q. S. Quek, "Channel sharing aided integrated sensing and communication: An energy-efficient sensing scheduling approach," *IEEE Trans. Wireless Commun.*, vol. 23, no. 5, pp. 4802–4814, May 2024.
- [9] J. Miguel Mateos-Ramos, C. Häger, M. Furkan Keskin, L. Le Magoarou, and H. Wymeersch, "Model-based end-to-end learning for multi-target integrated sensing and communication under hardware impairments," *IEEE Trans. Wireless Commun.*, vol. 24, no. 3, pp. 2574–2589, 2025.
- [10] Y. Wang, M. Tao, and S. Sun, "Cramér-rao bound analysis and beamforming design for integrated sensing and communication with extended targets," *IEEE Trans. Wireless Commun.*, vol. 23, no. 11, pp. 15987–16000, Nov. 2024.
- [11] X. Jing, F. Liu, C. Masouros, and Y. Zeng, "Isac from the sky: Uav trajectory design for joint communication and target localization," *IEEE Trans. Wireless Commun.*, vol. 23, no. 10, pp. 12857–12872, Oct. 2024.
- [12] Z. Lyu, G. Zhu, and J. Xu, "Joint maneuver and beamforming design for uav-enabled integrated sensing and communication," *IEEE Trans. Wireless Commun.*, vol. 22, no. 4, pp. 2424–2440, Apr. 2023.
- [13] H. Zhou, Y. Deng, X. Liu, N. Pappas, and A. Nallanathan, "Goal-oriented semantic communications for 6g networks," *IEEE Internet Things Mag.*, vol. 7, no. 5, pp. 104–110, Sep. 2024.
- [14] Y. Xu, H. Zhou, and Y. Deng, "Task-oriented semantics-aware communication for wireless uav control and command transmission," *IEEE Commun. Lett.*, vol. 27, no. 8, pp. 2232–2236, Aug. 2023.
- [15] W. Wu, Y. Yang, Y. Deng, and A. Hamid Aghvami, "Goal-oriented semantic communications for robotic waypoint transmission: The value and age of information approach," *IEEE Trans. Wireless Commun.*, vol. 23, no. 12, pp. 18903–18915, Dec. 2024.
- [16] J. A. Zhang, F. Liu, C. Masouros, R. W. Heath, Z. Feng, L. Zheng, and A. Petropulu, "An overview of signal processing techniques for joint communication and radar sensing," *IEEE J. Sel. Top. Signal Process.*, vol. 15, no. 6, pp. 1295–1315, Nov. 2021.
- [17] C. You and R. Zhang, "3d trajectory optimization in rician fading for uav-enabled data harvesting," *IEEE Trans. Wireless Commun.*, vol. 18, no. 6, pp. 3192–3207, Jun. 2019.
- [18] F. Liu, C. Masouros, A. Li, T. Ratnarajah, and J. Zhou, "Mimo radar and cellular coexistence: A power-efficient approach enabled by interference exploitation," *IEEE Trans. Signal Process.*, vol. 66, no. 14, pp. 3681–3695, Jul. 2018.
- [19] L. Pucci, E. Paolini, and A. Giorgetti, "System-level analysis of joint sensing and communication based on 5g new radio," *IEEE J. Sel. Areas Commun.*, vol. 40, no. 7, pp. 2043–2055, Jul. 2022.
- [20] J. T. Rodriguez, F. Colone, and P. Lombardo, "Supervised reciprocal filter for ofdm radar signal processing," *IEEE Trans. Aerosp. Electron. Syst.*, vol. 59, no. 4, pp. 3871–3889, Aug. 2023.
- [21] Q. Zhang, "Probability of resolution of the music algorithm," *IEEE Trans. Signal Process.*, vol. 43, no. 4, pp. 978–987, Apr. 1995.
- [22] M. Gasior and J. Gonzalez, "Improving fft frequency measurement resolution by parabolic and gaussian spectrum interpolation," in *Proc. AIP Conf.*, vol. 732, no. 1, 2004, pp. 276–285.
- [23] H. L. Van Trees, *Optimum array processing: Part IV of detection, estimation, and modulation theory*. Hoboken, NJ, USA: Wiley, 2002.
- [24] M. Gasior and J. Gonzalez, "Improving fft frequency measurement resolution by parabolic and gaussian spectrum interpolation," in *Proc. AIP Conf.*, vol. 732, no. 1, 2004, pp. 276–285.
- [25] T. S. Rappaport, G. R. MacCartney, M. K. Samimi, and S. Sun, "Wide-band millimeter-wave propagation measurements and channel models for future wireless communication system design," *IEEE Trans. Commun.*, vol. 63, no. 9, pp. 3029–3056, Sep. 2015.
- [26] D. Ciuonzo, G. Romano, and P. Salvo Rossi, "Performance analysis and design of maximum ratio combining in channel-aware mimo decision fusion," *IEEE Trans. Wireless Commun.*, vol. 12, no. 9, pp. 4716–4728, Sep. 2013.
- [27] J. Tranter, N. D. Sidiropoulos, X. Fu, and A. Swami, "Fast unit-modulus least squares with applications in beamforming," *IEEE Trans. Signal Process.*, vol. 65, no. 11, pp. 2875–2887, Jun. 2017.
- [28] M. Dobrevski and D. Skočaj, "Dynamic adaptive dynamic window approach," *IEEE Trans. Robot.*, vol. 40, pp. 3068–3081, 2024.
- [29] Z. Jian, Z. Liu, H. Shao, X. Wang, X. Chen, and B. Liang, "Path generation for wheeled robots autonomous navigation on vegetated terrain," *IEEE robot. autom. lett.*, vol. 9, no. 2, pp. 1764–1771, Feb. 2024.
- [30] H. Ghorbani, "Mahalanobis distance and its application for detecting multivariate outliers," *Facta Universitatis, Ser. Math. Informat.*, vol. 34, no. 3, pp. 583–595, Jun. 2019.
- [31] V. Mnih *et al.*, "Human-level control through deep reinforcement learning," *Nature*, vol. 518, no. 7540, pp. 529–533, Feb. 2015.
- [32] P. Luong, F. Gagnon, L.-N. Tran, and F. Labeau, "Deep reinforcement learning-based resource allocation in cooperative uav-assisted wireless networks," *IEEE Trans. Wireless Commun.*, vol. 20, no. 11, pp. 7610–7625, Nov. 2021.
- [33] K. Meng, Q. Wu, S. Ma, W. Chen, K. Wang, and J. Li, "Throughput maximization for uav-enabled integrated periodic sensing and communication," *IEEE Trans. Wireless Commun.*, vol. 22, no. 1, pp. 671–687, Jan. 2023.
- [34] X.-M. Zhang, Q.-L. Han, X. Ge, and B.-L. Zhang, "Accumulative-error-based event-triggered control for discrete-time linear systems: A discrete-time looped functional method," *IEEE/CAA J. Autom. Sin.*, vol. 12, no. 4, pp. 683–693, Apr. 2025.
- [35] G. Gallego, C. Cuevas, R. Mohedano, and N. García, "On the mahalanobis distance classification criterion for multidimensional normal distributions," *IEEE Trans. Signal Process.*, vol. 61, no. 17, pp. 4387–4396, Sep. 2013.
- [36] S. P. Boyd and L. Vandenberghe, *Convex Optimization*. Cambridge, U.K.: Cambridge Univ. Press, 2004.